BIOCHEMISTRY
including biophysical chemistry & molecular biology

Article

pubs.acs.org/biochemistry

# Understanding the Reaction Mechanism and Intermediate Stabilization in Mammalian Serine Racemase Using Multiscale Quantum-Classical Simulations

Neta Nitoker and Dan Thomas Major*

Department of Chemistry and the Lise Meitner-Minerva Center of Computational Quantum Chemistry, Bar-Ilan University, Ramat-Gan 52900, Israel

Supporting Information

**ABSTRACT:** Serine racemase (SerR) is a pyridoxal-5′-phosphate (PLP)-dependent enzyme catalyzing the racemization of L-Ser to D-Ser. In mammals, D-Ser is an endogenous coagonist required for the activation of *N*-methyl-D-aspartate receptors (NMDARs), thus making SerR a promising pharmaceutical target. However, mechanistic studies of SerR are scarce, and the details of the enzymatic racemization reaction are not fully understood. In the current study we elucidate the catalytic mechanism in SerR by employing combined multiscale classical/quantum simulations. The free energy profile of a model SerR racemization reaction is first calculated in the gas phase and in aqueous solution. To obtain the free energy profile for the enzymatic reaction, hybrid quantum mechanics/molecular mechanics molecular dynamics simulations in conjunction with umbrella sampling are performed. The results suggest that in SerR, similarly to the related enzyme alanine racemase, the unprotonated PLP-substrate intermediate is stabilized mostly due to solvation effects contributed by water molecules and active-site residues, as well as long-range electrostatic interactions with the enzyme environment. In addition to a deeper understanding of the racemization mechanism in SerR, based on our simulations we propose specific mutations, which might shift the SerR equilibrium in favor of either L-Ser or D-Ser. Finally, the current studies have produced catalytically competent forms of the rat and human enzymes, which may serve as targets for future docking studies and drug design.

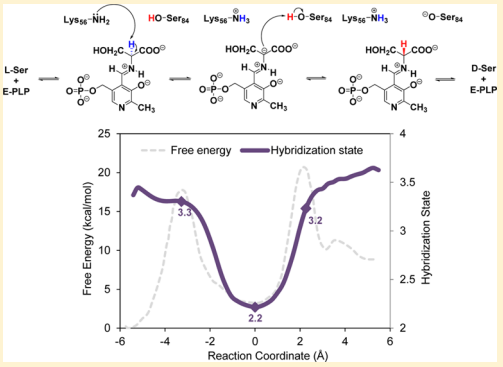


D-Amino acids were formerly thought to occur only in bacteria, where they play an important role in bacterial cell wall biosynthesis.[1] In the past two decades, high levels of D-Ser were discovered in many additional living organisms including yeast,[2] silk moth,[3] thale cress,[4] barley,[5] rice,[6] and importantly, in mammalian brain.[7]

D-Ser is synthesized from L-Ser in a reversible racemization reaction catalyzed by serine racemase (SerR), and consequently the role of SerR as a source of D-Ser is critical. This extensively studied D-amino acid has an essential role in the activation of *N*-methyl-D-aspartate receptors (NMDARs), which are present in the mammalian nervous system and mediate important physiological processes such as neurotransmission, synaptic plasticity, learning, and memory.[8] Recently, it has been demonstrated that NMDARs, D-Ser, and SerR are also expressed in keratinocytes in mammalian skin, where they are involved in epidermal differentiation and skin barrier formation.[9−11] Activation of NMDARs requires the binding of a coagonist to the glycine site of the receptor.[12] Recent studies[12−15] showed that D-Ser is up to three times more potent than Gly as a coagonist, suggesting that D-Ser is the physiological ligand for the glycine site. The importance of D-Ser has further been emphasized by studies suggesting that excessive activation of brain NMDARs can initiate medical conditions such as stroke, Alzheimer, Parkinson and Huntington's diseases,[16] and schizophrenic disorders in the case of poor activation.[17] Clearly, controlling the activity of NMDARs is of great importance. The use of glycine site blockers was found to be ineffective on NMDARs, causing heavy adverse effects such as hallucinations.[18] An alternative approach to reduce excessive activation of brain NMDARs is designing inhibitors targeting SerR, a task that would greatly benefit from structural and mechanistic understanding of SerR. Recent computational studies have suggested new inhibitors for mammalian SerR based on docking approaches.[19,20]

Like many other racemases, SerR employs pyridoxal-5′-phosphate (PLP) as a cofactor. In addition to racemization, SerR catalyzes the $\alpha,\beta$-elimination from L- and D-Ser generating pyruvate and ammonia.[21] By catalyzing these two reactions SerR controls the level of D-Ser in mammalian brain. While the physiological role of the elimination reaction has not been clarified yet, it is seemingly the main reaction catalyzed by SerR.[21,22]

The structural and mechanistic aspects of SerR have previously been studied using experimental tools. The catalytic racemization mechanism for *Schizosaccharomyces pombe* (*S.*

**Received:** August 7, 2014
**Revised:** November 21, 2014
**Published:** December 10, 2014





DOI: 10.1021/bi500984m
*Biochemistry* 2015, 54, 516−527

**Scheme 1. Racemization Reaction, L-Ser ⇄ D-Ser, Catalyzed by SerR**

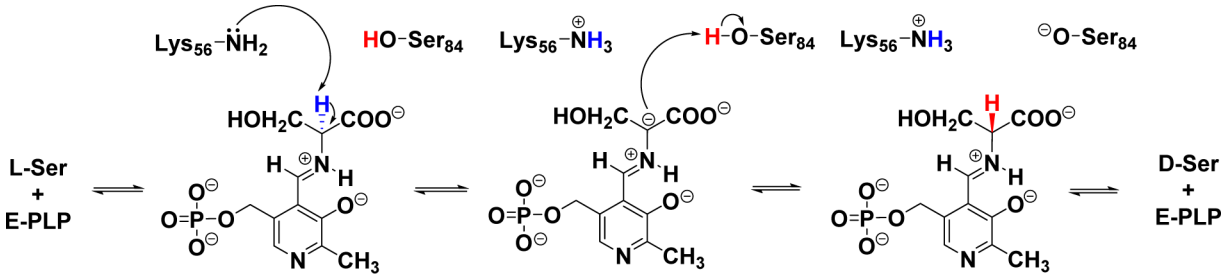


**Scheme 2. Model Reaction Studied in the Gas Phase and in Aqueous Solution**

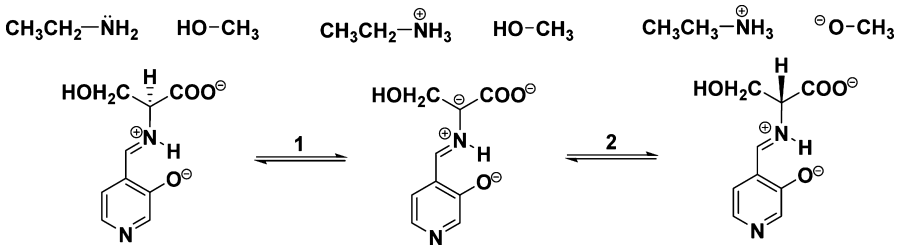


*pombe*) SerR was first proposed by Yoshimura and Goto,[2,23] based on the three-dimensional structure of the enzyme (PDB code 1WTC)[2] and on earlier mutagenesis studies.

On the basis of their studies, Yoshimura and Goto suggested that the racemization reaction in *S. pombe* SerR proceeds via a two-base mechanism and identified two catalytic residues, which are located on opposite sides of the PLP-conjugated plane - Lys57 (Lys56 in mammalian SerR), which acts as a base in the L-Ser → D-Ser reaction, and Ser82 (Ser84 in mammalian SerR), which acts as an acid. The mechanism suggested for mammalian SerR[24] is in line with the mechanism proposed for *S. pombe* SerR and is presented in Scheme 1. The L → D isomerization commences with the PLP cofactor in the internal aldimine form, wherein a Schiff-base connects the cofactor to the enzyme via Lys56. Subsequently, L-Ser binds to SerR followed by a transaldimination, forming a Schiff-base between the substrate and the cofactor (external aldimine) while releasing Lys56. L-Ser of the resulting external aldimine is deprotonated at the C$\alpha$ position by Lys56 and a carbanionic intermediate is formed. Next, C$\alpha$ is protonated by Ser84 on the opposite side of the PLP ring plane, to form D-Ser which is covalently linked to PLP, and finally the substrate, D-Ser, is displaced by Lys56 via another transaldimination.[23] Structures of the related *Bacillus stearothermophilus* alanine racemase (AlaR)[25−27] and *Dictyostelium discoideum* SerR[23] further support the proposed mechanism.

In most PLP-dependent enzymes, the carbanionic intermediate formed in the reaction is stabilized by delocalization of the negative charge to the PLP "electron sink".[28] This stabilization is achieved in cases where the PLP pyridine nitrogen ($pK_a \sim 5.8$)[29] is protonated, a feature that makes it more electrophilic. In SerR, the presence of a nonacidic residue (Ser, that has a side-chain $pK_a$ of ~14),[30] in close proximity to the pyridine nitrogen, most likely keeps it unprotonated.[31,32] In Trp synthase, a Ser residue interacts with the pyridine nitrogen similarly to the case of SerR, and NMR experiments confirmed that this ring nitrogen remains unprotonated.[33] The stabilization of the carbanionic intermediate is therefore probably achieved without the help of an electron sink.[23]

Computational studies regarding the protonation state of the pyridine in AlaR were performed by Major, Gao, and coworkers.[34−37] In AlaR the PLP pyridine nitrogen is in close proximity to Arg219, suggesting that the nitrogen atom is unprotonated. These studies showed that the stabilization of the carbanion intermediate in AlaR is achieved mostly due to solvation effects contributed by water molecules and active-site residues, as well as long-range electrostatic interactions with the enzyme environment. It was further shown that for the Arg219Glu mutant form of AlaR, where the pyridine nitrogen is protonated, the enhanced stabilization of the intermediate is due to an electron sink effect.[36] In this work it was also shown that the enhanced stabilization of the carbanion intermediate facilitates transamination in the mutant enzyme. It is of great interest to understand the nature of the stabilization mechanism taking place in SerR.

Here, the reaction mechanism in SerR is addressed via a combined quantum mechanical and molecular mechanical (QM/MM) approach.[38−40] The potential of mean force (PMF) for the racemization in SerR is obtained from umbrella sampling (US) molecular dynamics (MD)[41,42] simulations. To elucidate the catalytic power of SerR, the results obtained for the enzymatic reaction are compared with the free energy profiles of a model reaction calculated in the gas phase and in aqueous solution. The contribution of individual enzyme residues to catalysis is further expounded.

## 2. METHODOLOGY

**QM Calculations in Gas and Solution Phases.** A two-step model racemization reaction (Scheme 2) was studied in the gas phase and in aqueous solution. Initially, the geometries of the individual molecules were optimized in the gas phase, and their thermochemical properties were calculated using four different QM methods, including two density functional theory (DFT) methods and two semiempirical (SE) methods. The DFT methods used are M06[43] and mPW1PW91[44] with the 6-31+G(d,p) basis set,[45] and the SE methods are the Austin Model 1 (AM1)[46] and AM1 with specific reaction parameters (AM1-SRP). The latter model was developed particularly for



DOI: 10.1021/bi500984m
*Biochemistry* 2015, 54, 516−527

AlaR, and was shown to be accurate for other racemases as well.[34−36,47,48]

To establish the accuracy of AM1-SRP for the L-Ser ⇄ D-Ser racemization, the gas-phase reaction free energies were calculated using the Gibbs free energy values obtained for the individual molecules with the four methods mentioned above.

To calculate the full free energy profile in the gas and solution phases, the two steps of the reaction (Scheme 2) were treated separately, and each stationary point was presented as a complex of two molecules (in each step of the reaction, the complex was composed of the proton donor and acceptor). Because of the difficulty in optimizing the geometry of the complexed structures, especially in the gas phase, constraints were applied on specific distances, angles, and dihedrals (see Table S3 of the Supporting Information). The geometry of each complex was optimized in the gas phase and in solution using AM1-SRP, and the thermochemical properties were calculated, from which the free energy barriers and reaction free energies of the two steps were calculated. The solvent used for solution-phase calculations was water, and the integral equation formalism polarizable continuum model (IEF-PCM)[49−52] was employed.

All calculations in the gas and solution phases were performed using the Gaussian09 program.[53]

**QM/MM Simulations of SerR.** *Construction of the Michaelis Complex.* The X-ray crystal structures of human and rat SerRs, in the absence and presence of the orthosteric inhibitor malonate, were recently published by Smith and co-workers.[24] Human and rat SerRs are homodimers with ca. 90% sequence identity, wherein each monomer of the human enzyme contains 346 amino acid residues, and the rat enzyme contains 339 amino acids in each monomer. Both structures have an overall fold typical of $\beta$-family PLP-dependent enzymes, with a large domain, in which the active site is located, and a flexible small domain.

The enzyme contains a structurally important divalent metal ion ($Mg^{2+}$, $Ca^{2+}$, or $Mn^{2+}$), which is necessary for complete SerR activity.[54,55] Its location distal to the active site suggests an indirect catalytic effect, such as facilitating SerR folding by causing a conformational change in the ternary structure of SerR, thereby increasing its activity.[56] Nucleotides (mainly the complex Mg·ATP) also increase the activity of SerR under physiological conditions.[21,55,57] Despite their importance for SerR function, the published crystal structures of mammalian SerRs do not contain a nucleotide ligand.[24] However, an ATP analogue, 5-adenylyl methylenediphosphate (AMP-PCP), has been crystallographically detected in *S. pombe* SerR, where it is complexed with $Mg^{2+}$.[2] Its binding site is located at the intersection between the domain interface and the monomer interface. Upon binding of a nucleotide to this allosteric site, a hydrogen bond network, which is mediated by SerR residues, is formed between the nucleotide and the PLP cofactor. It has been suggested that when a substrate binds to the cofactor, the H-bond network might change to fine-tune the position of key residues in the active site, resulting in increased SerR activity.[2]

The rat SerR crystal structure (pdb code 3L6C) was used to construct the initial configuration for our study. The original ligand, malonate, was deleted and replaced by the substrate L-Ser. The substrate was manually linked to the PLP cofactor, replacing Lys56, to create the external aldimine Michaelis complex. The carboxylate was constructed in two conformations (syn or anti relative to the PLP oxyanion). Subsequent free energy simulations indicated that the syn conformer is the preferred one and only this state is considered below. Missing crystallographic residues (1 and 324−339 in monomer A; 1−3, 67−75 and 325−339 in monomer B) were added manually to the original structure. The residues missing at the N-terminus and C-terminus were added in an extended conformation. To relax the conformations of the added residues and substrate, geometry minimization and MD simulations were performed on these parts of the enzyme, while the remaining regions were kept fixed. Residues 67−75 of monomer B, which constitute a loop region, were folded to a minimum energy conformation using the *Loop Refinement* tool of Discovery Studio (DS) 3.0 (Accelrys Inc.). An Mg·AMP-PCP ligand was extracted from *S. pombe* SerR (1WTC) and docked into the allosteric site of rat SerR after superimposing both crystal structures. Then, AMP-PCP was modified to ATP, and the Mg·ATP complex was minimized. A model for human SerR was constructed as well (using pdb structure 3L6B), following the same protocol as for rat SerR.

All modifications and simulations mentioned in the above paragraph were performed using DS 3.0.

The coordinates of hydrogen atoms of the protein and water were determined using the HBUILD facility in the CHARMM program.[58,59] The protonation states of ionizable residues were set according to hydrogen bond schemes and are suitable for pH 8, which is the experimentally relevant pH.[24] The possible protonation states of His residues (protonated on N$\varepsilon$, N$\delta$, or both) were determined in the same manner, while surface His residues were treated as protonated. Nine sodium counterions were added in random positions around the negatively charged enzyme to obtain a net-neutral system.[60]

*Hybrid QM(AM1-SRP)/MM Potential Energy Surface.* The proton transfer reactions in SerR were treated with a hybrid QM/MM potential energy surface[38]

$$\hat{H} = \hat{H}_{QM} + \hat{H}_{MM} + \hat{H}_{QM/MM} \quad (1)$$

The QM/MM partitioning scheme is shown in Figure 1. The QM region, which was treated by AM1-SRP, consisted of 49

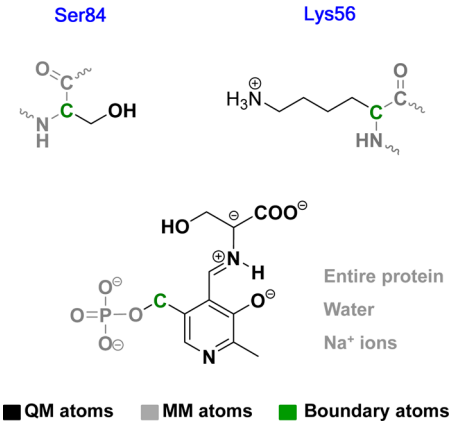


**Figure 1.** QM/MM partitioning scheme used for SerR simulations.

atoms in monomer A: Lys56, Ser84, and the Ser-PLP cofactor, excluding the phosphate moiety. The Generalized Hybrid Orbital (GHO)[61] method was employed for the C$\alpha$ atoms of Lys56 and Ser84, and C5A (phosphorylated carbon) of the PLP. The MM region contained the rest of the system (including water) and was treated with the CHARMM36 force



DOI: 10.1021/bi500984m
*Biochemistry* 2015, 54, 516−527

field.[62−64] Interactions between the QM and MM regions were treated using an electrostatic embedding scheme.

*Potential of Mean Force Simulations.* The classical PMF as a function of the reaction coordinate $\zeta$ is defined as

$$W(\zeta) = -RT\ln \rho(\zeta) + C \quad (2)$$

where $\rho$ is the unbiased probability density along the reaction coordinate $\zeta$, $R$ is the gas phase constant, $T$ is the temperature, and $C$ is a normalization constant.[65,66]

The PMF of the L-Ser → D-Ser reaction was determined as a function of three reaction coordinates. The first coordinate, $\zeta_1$, is defined as the difference between the C$\alpha$-H bond length (breaking during deprotonation of C$\alpha$ by Lys56) and the H−N bond length (forming during deprotonation). The second coordinate, $\zeta_2$, is defined as the difference between the O−H bond length (breaking during protonation of C$\alpha$ by Ser84) and the H−C$\alpha$ bond length (forming during protonation). A schematic description of $\zeta_1$ and $\zeta_2$ is presented in Figure 2. The

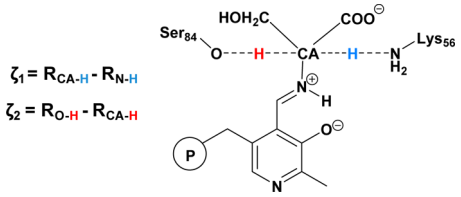


**Figure 2.** Depiction of the first two reaction coordinates employed in the SerR simulations.

third coordinate, $\zeta_3$, is the hybridization state of the C$\alpha$ atom. During racemization, the values of this coordinate fluctuate between 2 ($sp^2$ hybridization) and 3 ($sp^3$), and are determined geometrically as follows:

$$\zeta_3 = 2 + 3L \quad (3)$$

where $L$ is the distance between C$\alpha$ and the plane defined by its substituents—the Schiff base, the carboxylate group and the R group of the substrate.[67−69]

A three-dimensional PMF profile was obtained by employing adaptive umbrella sampling (US) MD simulations,[41,70] in which the reaction coordinate is divided into windows that are sampled in separate simulations. A biasing potential was applied to $\zeta_1$ and $\zeta_2$ in order to improve the sampling of regions that are high in energy, while $\zeta_3$ was treated as a spectator coordinate. The free energies of the separate simulation windows along the reaction coordinate were combined using the weighed histogram analysis method (WHAM),[71] to obtain the PMF profile as a function of the first two reaction coordinates. A one-dimensional minimum free energy path was obtained from the 2D PMF using the string method.[68,72] Additionally, the hybridization state of the C$\alpha$ atom throughout the reaction, i.e., $\zeta_3$, was sampled as a function of $\zeta_1$ and $\zeta_2$.

Prior to commencing MD simulations, the system was embedded in a cubic box of 85 × 85 × 85 Å$^3$, containing 166 877 water molecules. Periodic boundary conditions[60] were employed in conjunction with the Ewald summation method for electrostatic interactions.[73] The system was relaxed employing a stepwise minimization protocol before running MD simulations. The isothermal−isobaric ensemble (NPT) was employed at 1 atm and 298 K. The MD simulations entailed slowly heating the system from 48 to 298 K over the course of 25 ps, followed by equilibration at 298 K for 1 ns. Each window was further equilibrated for 200 ps and sampled for about 375 ps. Sampling was continued until the PMF was invariant to within approximately ±1.0 kcal/mol, which is the expected statistical error in such simulations.[65]

*Nuclear Quantum Effects.* The PMF is obtained from classical mechanics MD simulations, which are based on Newton's equations of motion (henceforth CM PMF). Therefore, it does not include nuclear quantum effects (NQE), such as zero-point energy and tunneling, which are required for the determination of accurate free energy barriers in proton transfer reactions. We employed bisection centroid path integral (PI) simulations[74−78] to evaluate the NQE on the computed PMF (henceforth QM PMF). In the PI simulation, each of the quantized atoms (donor and acceptor heavy atoms and the transferring proton) was represented by a ring of 32 quasi-particles or beads, wherein their geometrical center (centroid) is constrained to the classical position. For each of the two racemization steps, about 30 000 classical configurations were extracted from the MD trajectory. For each such configuration, 10 Monte Carlo free particle sampling steps were performed.

## 3. RESULTS AND DISCUSSION

**Model Gas-Phase QM Calculations.** The computed gas-phase free energies for the L-Ser → D-Ser model reaction are presented in Table 1. At all levels, the reaction is highly

**Table 1. Reaction Free Energies (kcal/mol) Obtained for the L-Ser → D-Ser Model Reaction in the Gas Phase**

| | M06 | mPW1PW91 | AM1 | AM1-SRP |
|---|---|---|---|---|
| $\Delta G_{reaction}$ | 166.38 | 167.22 | 173.17 | 165.39 |

unfavorable in the gas-phase, due to the formation of ions. A comparison between the results obtained from AM1-SRP and from the DFT methods shows a maximum difference of only 1.8 kcal/mol, suggesting that the SRP model developed for the AlaR reaction is equally applicable to the SerR reaction. The errors obtained with the original AM1 method are considerably higher.

The accuracy of the AM1-SRP model for serine racemization was further verified by our gas-phase calculations of proton affinities (Table S4 of the Supporting Information).

**Racemization Reaction.** *Free Energy Simulations in SerR.* The current simulations employ a hybrid QM/MM potential energy surface to allow an explicit treatment of the electronic degrees of freedom necessary to describe bond breaking and forming. In conjunction with classical, Newtonian, MD simulations and US, this approach gives the classical free energy reaction profiles (i.e., CM PMF). Additionally, to account for the quantum nature of the transferring protons, such as zero-point energy and tunneling, we employ a PI simulation method. This latter approach yields quantum free energy profiles (i.e., QM PMF), which are based on the CM PMF combined with a nuclear quantum correction.

The CM PMF profiles of the enzymatic racemization reaction, as a function of $\zeta_1$, $\zeta_2$, and $\zeta_3$, were obtained from Newtonian MD simulations in conjunction with US. The one- and two-dimensional PMF profiles for rat SerR, as a function of the first two coordinates, are presented in Figure 3. Initial results for human SerR, which are very similar to those for the rat enzyme, are presented in Figure S2, Supporting Information. A full analysis of the human form will be the focus of future work. In constructing the 1D plot (Figure 3b),


DOI: 10.1021/bi500984m
*Biochemistry* 2015, 54, 516−527

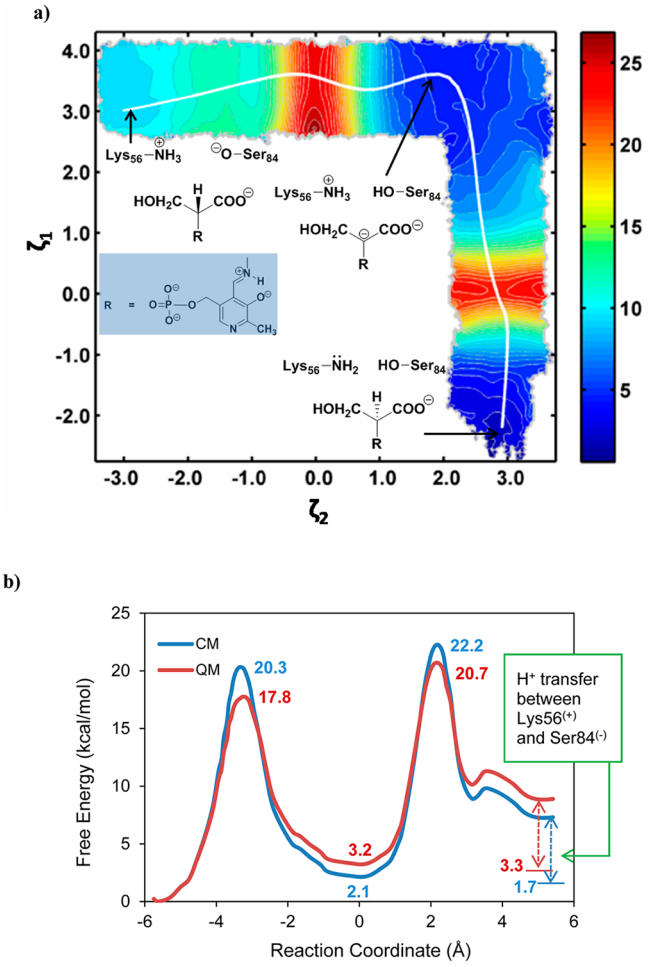


**Figure 3.** (a) Classical 2D PMF surface (kcal/mol) as a Function of $\zeta_1$ and $\zeta_2$, (b) CM and QM 1D PMF surface for the SerR catalyzed racemization reaction.

we shifted the reaction coordinate by approximately −3 and 3 Å for the first and second reaction steps, respectively, to display both reaction profiles in the same figure. Additionally, we set the relative free energy of the reactant state to zero and the free energy values of the deprotonation intermediate to be identical for both reaction steps. The CM free energy barrier, as obtained from the corresponding PMF profiles, is 22.2 kcal/mol for the L → D direction (right bottom to upper left in the 2D plot, left to right in the 1D plot) and 18.2 kcal/mol for the D → L direction (upper left to right bottom in 2D plot, right to left in 1D plot). We note that the barriers in both directions are expected to be similar in racemase reactions. The total reaction free energy for the L → D reaction is 7.3 kcal/mol. This imbalance can be explained by the protonation states of the catalytic residues at the end of the L → D reaction (both Lys56 and Ser84 are charged). Since the p$K_a$ of the Lys side chain is much lower than the p$K_a$ of the Ser OH group, a final $H^+$ transfer from Lys56 to Ser84 will further reduce the free energy of the products by ∼5.6 kcal/mol, which is the energy required for protonation between the two residues. Including this final protonation, the free energy of the products is ∼1.7 kcal/mol, and the CM barrier in the D → L direction will be about 20.5 kcal/mol. Addition of NQE to the CM PMF to produce the QM PMF, reduces the L → D free energy of activation by 1.5 kcal/mol, giving a barrier of 20.7 kcal/mol. In the reverse direction, the QM correction is −3.1 kcal/mol, giving a barrier of 17.4 kcal/mol. Experimental kinetic data are not available for rat SerR in complex with an allosteric ATP ligand. Therefore, our results were compared to kinetic data obtained for rat SerR in the absence of this ligand.[79] The calculated free energies of activation are in good agreement with the experimental values, as can be seen in Table 2. Inclusion of ATP would probably

**Table 2. Free Energy Barriers (kcal/mol) Obtained for the Enzymatic L-Ser ⇄ D-Ser Reaction**

| | $\Delta G^{\ddagger}$ | | |
|---|---|---|---|
| | CM | QM | exp[a] |
| L-Ser → D-Ser | 22.22 | 20.69 | 19.13 |
| D-Ser → L-Ser | 20.48 | 17.37 | 18.26 |

[a]Eyring equation was used to translate experimental $k_{cat}$ values to $\Delta G^{\ddagger}$ values. The $k_{cat}$ values are taken from ref 79.

have reduced the experimental barriers by 0.5−1.5 kcal/mol, according to experimental results obtained for mouse SerR in the presence and absence of ATP.[80] Our results suggest that the unprotonated form of the pyridine ring in PLP is likely the correct protonation state for this reaction, as protonation of the pyridine ring results in large changes in the free energy profiles.[34−36] We speculate that the pyridine protonated form of SerR may catalyze the $\alpha,\beta$-elimination from L- and D-Ser generating pyruvate and ammonia. This can be tested by mutating Ser313, which interacts with the pyridine nitrogen, to an acidic residue in order to obtain a protonated pyridine, as was previously done in our group for AlaR.[36]

We observe some secondary features in the free energy profile in Figure 3b (at the end of the L → D reaction with a local minimum at $\zeta \approx 3$ Å). A possible explanation could be an observed rotation of ∼120° around the C$\delta$−C$\gamma$ bond of Lys56, which places the -$NH_3^+$ group in a position where the hydrogen bond with the carbonyl moiety of Pro153 is significantly shorter, and as a result the free energy is reduced.

*Hybridization State of Cα.* Figure 4 shows the hybridization state of the substrate C$\alpha$ atom, as well as the free energy, as a function of the other two reaction coordinates. We note that the calculated hybridization states at the minima along the PMF are not identical to the formal ones, due to the geometric definition used for hybridization and numerical noise inherent

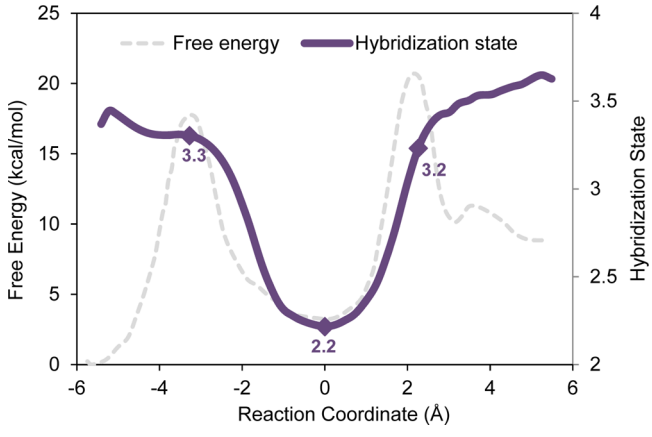


**Figure 4.** Hybridization state of C$\alpha$ (solid) and the free energy (dashed) as a function of the L-Ser → D-Ser reaction coordinate. The marked dots are the hybridization state at the transition states and the intermediate (smoothed data).



DOI: 10.1021/bi500984m
*Biochemistry* 2015, 54, 516−527

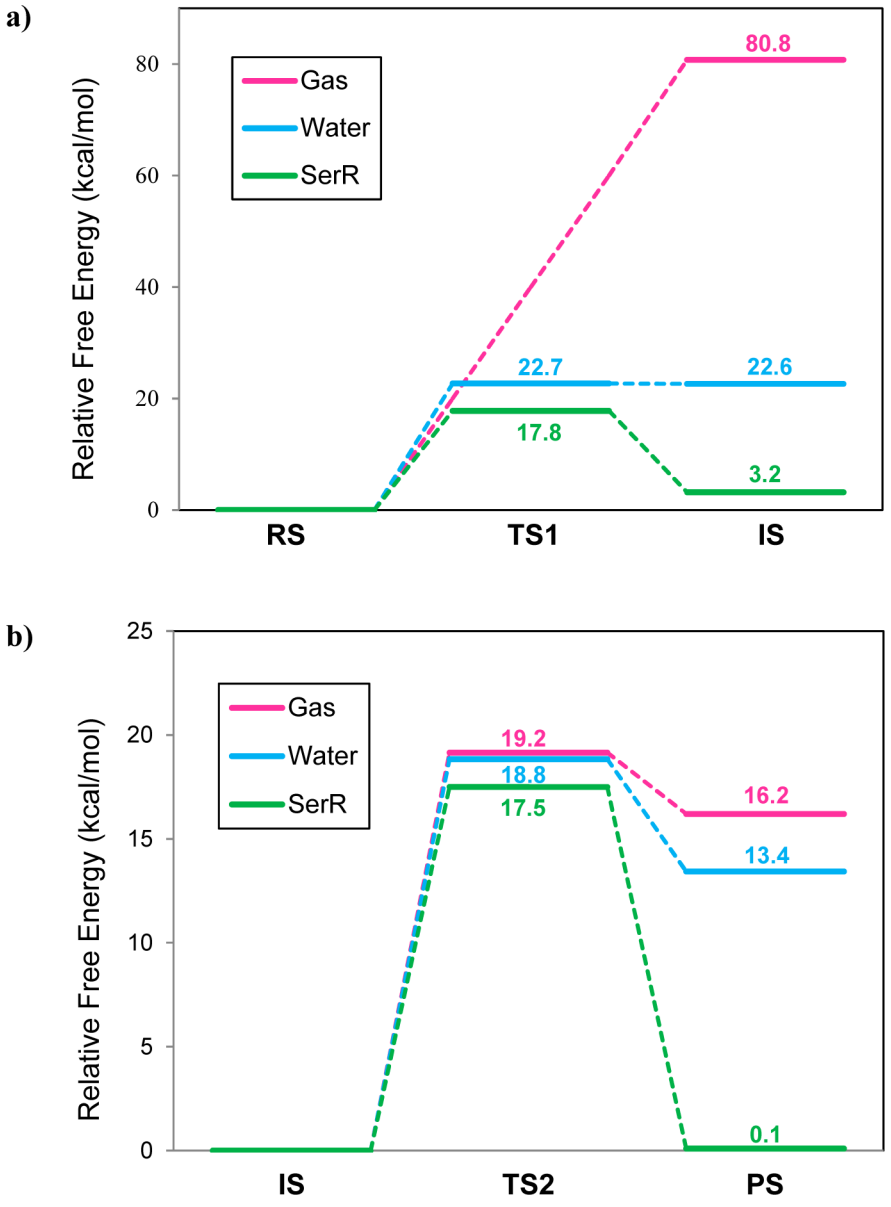


**Figure 5.** Free energy profiles for the L-Ser → D-Ser Racemization in the gas phase, water and SerR: (a) The first reaction step (reactant state through intermediate state). (b) The second step (intermediate state through product state).

to MD simulations. By inspecting Figure 4, it can clearly be seen that during the first reaction step, C$\alpha$ undergoes rehybridization from $sp^3$ to $sp^2$, and in the second step the hybridization state changes back to $sp^3$. These findings are in line with the L-Ser → D-Ser reaction mechanism in which the tetrahedral C$\alpha$ of L-Ser is first deprotonated to form a planar anionic intermediate (due to the formation of a C$\alpha$=N double bond), and in the second step the serine anion is reprotonated to form a tetrahedral D-Ser. When comparing the rehybridization plot with the free energy plot, it can be seen that in both the first and second transition states (TSs), the hybridization state of C$\alpha$ has hardly changed in comparison with the reactant state (RS) and product state (PS), respectively, and is still ~3. This suggests that the C$\alpha$ rehybridization is much slower than the progress of the proton transfer. A similar lag has been encountered in other enzymatic reactions which involve carbon rehybridization[67,81] and is an example of the principle of nonperfect synchronization.[82]

*A Comparison between Free Energy Profiles in Gas Phase, Water and SerR.* In Figure 5, the free energy profiles for the two reaction steps in SerR are compared with the profiles obtained from gas and solution-phase calculations. While the initial proton abstraction (Step 1, Figure 5a) is highly unfavorable in the gas phase, and a TS is not found, the inclusion of water as a solvent greatly stabilizes the ionic products of the C$\alpha$ deprotonation, and lowers the $\Delta G$ of the first step by ~58 kcal/mol, with a barrier of 22.7 kcal/mol. The reaction is still endergonic, possibly due to the negative charge formed in this step, which accumulates around the cofactor PLP moiety, and the resulting electrostatic repulsion between the PLP oxyanion and the carboxylate group of the substrate. In SerR, this repulsion is reduced due to strong interactions of the carboxylate group of the substrate with Asn86, His87, and Ser83. Therefore, in SerR, the $\Delta G$ is only 3.2 kcal/mol, with a $\Delta G^{\ddagger}$ of 17.8 kcal/mol. The second step (Figure 5b) is unfavorable in the gas phase because the delocalized charge of PLP-$Ser^-$ is neutralized, and a localized charge is formed on an


DOI: 10.1021/bi500984m
*Biochemistry* 2015, 54, 516−527

oxygen atom (Scheme 2). However, the reaction $\Delta G$ is much lower in comparison to the first step because the electrostatic repulsion on PLP-Ser is reduced once C$\alpha$ is protonated. In water, a similar free energy barrier is obtained although the reaction free energy is reduced. In the enzyme environment, the charged species are stabilized due to interactions with surrounding residues as well as water molecules, and $\Delta G$ is reduced to almost zero, with a barrier of 17.5 kcal/mol.

These findings emphasize the stabilizing effect of solvent on the L-Ser → D-Ser isomerization in the presence of a PLP cofactor. Importantly, the enzyme reaction occurs via a stepwise mechanism with a distinct intermediate PLP-substrate carbanion species. Our results are in line with the results obtained from our previous AlaR studies,[34,35] which showed that the major contribution to stabilization of the carbanion intermediate formed in the L-Ala ⇄ D-Ala reaction is provided by solvation effects due to water and active-site residues, and long-range electrostatic interactions with the enzyme.

*Structural Analysis of the SerR Active Site.* In Table 3 we present important geometrical features in the rat SerR active site, including H-bond donor−acceptor distances between the cofactor-substrate complex, the catalytic residues and other key residues that interact with the reacting complex, at five states throughout the reaction: RS (Figure 6), first TS ($TS_1$), intermediate state (IS), second TS ($TS_2$), and PS. In the L → D half-reaction, the distance between the Ser-PLP C$\alpha$ (referred to as CA in Table 3) atom and the Lys56 N$\zeta$ (NZ in Table 3) atom is 4.0, 2.7, and 4.5 Å for the RS, $TS_1$, and IS, respectively, while the distance between C$\alpha$ and the Ser84 oxygen atom (OG2) remains in the narrow range between 4.0 and 4.4 Å. In the next step of the reaction, the CA−NZ distance hardly changes, while the CA−OG2 distance changes from 4.0 (IS) to 2.6 ($TS_2$) to 4.4 Å (PS). Throughout the reaction, the PLP pyridine nitrogen (N1) interacts with Ser313 via a short H-bond that ranges between 2.7 and 2.9 Å. The H-bond between the pyridine oxyanion (O3A) and the side chain (ND2) of Asn86 remains intact throughout the reaction (2.8−3.0 Å). Other interactions that remain firm are H-bonds formed between the substrate carboxylate oxygens (O and OXT) and the Ser83 side chain (2.8−3.0 Å), as well as the amide backbone moieties of Ser84, Gly85, Asn86, and His87. The catalytic Lys56, which becomes charged during the course of the reaction, is stabilized mainly via the backbone carbonyl of Pro153. This interaction is weakened only at $TS_1$, where the $NH_2$ group of Lys56 gets closer to the substrate for protonation. The Ser84-$O^-$ ion, on the other hand, is stabilized mostly by water molecules located in the active site and are not included in Table 3. All interactions between SerR and the PLP-phosphate moiety (not included in Table 3) remain tight throughout the reaction.

**Table 3. Average Distances (Å) for Selected Hydrogen Bonding Interactions in the Active Site, at the Reactant, Transition, Intermediate and Product States (L → D direction)[a]**

| | | distance | | | | |
|---|---|---|---|---|---|---|
| donor | acceptor | RS | $TS_1$ | IS | $TS_2$ | PS |
| ND2, Asn86 | O3A, PLP | 2.90 | 3.04 | 2.82 | 2.77 | 2.98 |
| OG, Ser83 | OXT, PLP | 2.93 | 2.95 | 2.78 | 2.77 | 2.80 |
| OG, Ser313 | N1, PLP | 2.71 | 2.67 | 2.73 | 2.87 | 2.65 |
| N, Ser84 | OXT, PLP | 3.57 | 3.55 | 2.90 | 2.95 | 2.93 |
| N, Gly85 | O, PLP | 4.08 | 3.93 | 3.36 | 3.88 | 3.89 |
| N, Gly85 | OXT, PLP | 3.96 | 3.83 | 3.71 | 2.96 | 4.17 |
| N, Asn86 | O, PLP | 3.92 | 4.09 | 3.02 | 3.52 | 3.26 |
| N, His87 | O, PLP | 3.44 | 3.79 | 3.15 | 2.87 | 2.94 |
| NZ, Lys56 | O, Pro153 | 3.60 | 4.04 | 3.02 | 2.94 | 2.46 |
| CA, PLP | NZ, Lys56 | 3.98 | 2.73 | 4.46 | 4.81 | 4.79 |
| OG2, Ser84 | CA, PLP | 4.34 | 4.39 | 4.01 | 2.60 | 4.37 |

[a]The structures have been averaged over 5000 configurations. Standard deviations in the average distances are 0.1−0.4 Å.

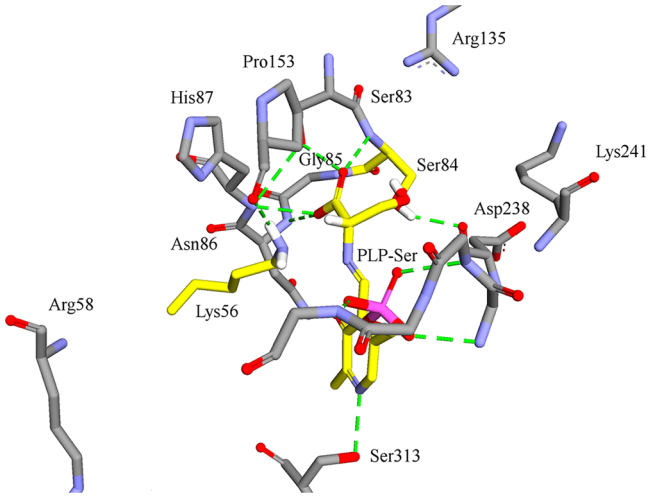


**Figure 6.** Active-site interactions of Ser-PLP with its surrounding residues, at the reactant state (Ser-PLP and the two catalytic residues are colored with carbon atoms in yellow).

*Analysis of ATP Interactions.* In addition to the analysis of geometrical features in the active site of SerR, interactions between the Mg·ATP ligand and its surroundings were analyzed throughout the L-Ser → D-Ser racemization. The H-bond donor−acceptor distances are listed in Table 4. As can be deduced from the data, the nucleotide is held firmly in place through short hydrogen bonds with nine amino acid residues (Figure 7), which remain intact throughout the reaction. The ribose hydroxyl groups interact with Gln89, Asn316, and Lys279′ (a prime indicates residues from the second subunit), and the triphosphate oxygen atoms accept H-bonds from Thr52, Arg277′, Lys51, Ser31′, Ser32′, and His24. These interactions, excluding the ones with Gln89 and His24, are conserved in *S. pombe* SerR, holding the AMP-PCP ligand in place. There is also a good agreement with the ATP binding site of human SerR presented by Jirásková et al.,[83] in which eight of the nine residues stabilizing the ATP ligand in rat SerR, are conserved, while the interactions with two residues (Gly53 and Tyr121) in human SerR are absent in the rat enzyme.

Additionally, the H-bond network between the ATP ligand and the PLP cofactor was examined throughout the reaction. The O3′ atom of PLP is linked to the ribose hydroxyl groups and the $\alpha$-phosphate group of ATP via an H-bond network formed by Asn86, Glu283, Asn316, and Thr52 (Figure 7). The donor−acceptor distances of the H-bonds creating the network are specified in Table 4. Throughout the reaction, the interaction network remained intact. This network is similar to the interaction network in *S. pombe* SerR, except for Gln87 of *S. pombe* SerR (Gln89 in rat SerR), which is involved in the network via interactions with water molecules, while Gln89 of rat SerR takes part in stabilizing the ATP ligand, but is not involved in the H-bond network between ATP and PLP.


DOI: 10.1021/bi500984m
*Biochemistry* 2015, 54, 516−527

**Table 4. Average Distances (Å) for Selected Hydrogen Bonding Interactions in the ATP Binding Site, and Between ATP and the PLP cofactor, at the Reactant, Transition, Intermediate, and Product States(L → D Direction)[a]**

| | | distance | | | | |
|---|---|---|---|---|---|---|
| donor | acceptor | RS | $TS_1$ | IS | $TS_2$ | PS |
| O2′, ATP | OE1, Gln89 | 2.70 | 2.71 | 2.71 | 2.71 | 2.67 |
| NZ, Lys279′ | O3′, ATP | 3.01 | 3.01 | 3.07 | 3.03 | 3.15 |
| NH2, Arg277′ | O2A, ATP | 2.94 | 2.93 | 3.06 | 2.99 | 3.04 |
| NE, Arg277′ | O1B, ATP | 2.77 | 2.77 | 2.75 | 2.75 | 2.76 |
| NH2, Arg277′ | O1B, ATP | 3.04 | 2.93 | 2.82 | 2.83 | 2.83 |
| NZ, Lys51 | O3B, ATP | 2.86 | 2.87 | 2.85 | 2.82 | 2.91 |
| OG, Ser31′ | O1G, ATP | 2.65 | 2.64 | 2.65 | 2.67 | 2.65 |
| OG, Ser32′ | O2G, ATP | 2.65 | 2.66 | 2.68 | 2.66 | 2.71 |
| N, Ser32′ | O2G, ATP | 2.75 | 2.75 | 2.76 | 2.81 | 2.75 |
| NE2, His24 | O3G, ATP | 2.71 | 2.69 | 2.67 | 2.70 | 2.68 |
| ND2, Asn86 | O3A, PLP | 2.95 | 3.03 | 2.80 | 2.92 | 2.98 |
| ND2, Asn316 | OD1, Asn86 | 3.31 | 3.35 | 3.33 | 3.30 | 3.23 |
| O2′, ATP | OD1, Asn316 | 3.43 | 3.58 | 3.45 | 3.32 | 3.31 |
| O3′, ATP | OD1, Asn316 | 2.83 | 2.89 | 2.85 | 2.80 | 2.89 |
| ND2, Asn86 | OE2, Glu283 | 2.89 | 2.82 | 2.87 | 2.82 | 2.82 |
| N, Asn316 | OE2, Glu283 | 3.21 | 3.64 | 3.33 | 3.35 | 3.64 |
| ND2, Asn316 | O, Thr52 | 2.90 | 2.92 | 2.94 | 2.92 | 2.84 |
| N, Thr52 | O1A, ATP | 2.74 | 2.72 | 2.74 | 2.86 | 2.67 |

[a]The structures have been averaged over 5000 configurations. Standard deviations in the average distances are 0.1−0.4 Å.

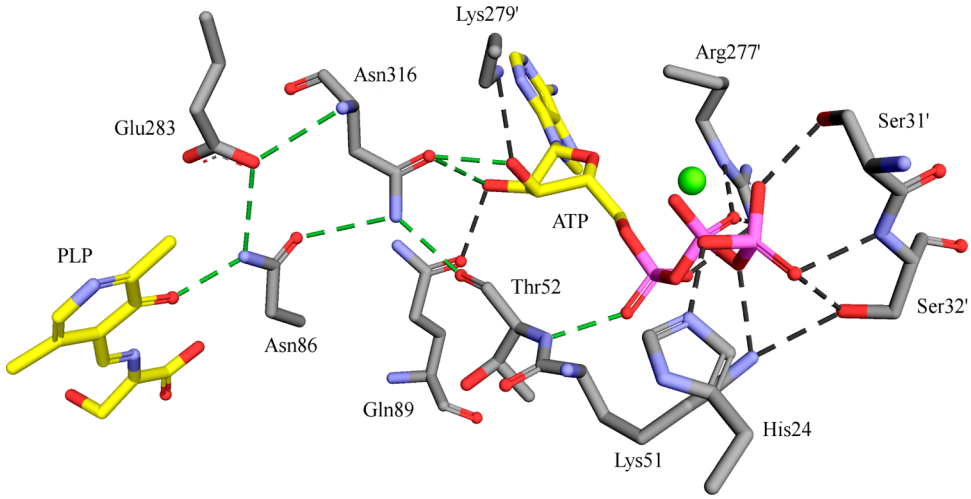


**Figure 7.** Hydrogen bond network between the PLP cofactor and the ATP ligand (the interactions in green are the ones involved in the H-bonds network).

**Roles of Active-Site Residues in SerR Catalysis.** The roles of active-site residues, important to binding and to catalysis in SerR, were examined by an interaction energy decomposition analysis, an approach that has been previously used to study a number of enzymes.[84−86] This method involves sequential charge annihilation to determine the average interaction energies, starting from the residues closest to the active site. Although this kind of analysis depends on the division of QM and MM regions, the results can provide valuable information regarding binding interactions and TS stabilization. We used the structures corresponding to the reactant state (RS), first transition state (TS), and intermediate state (IS), which were saved during our umbrella-sampling MD simulations. For each step, a total of ca. 1000 configurations were averaged. For each configuration, the MM charges of each amino acid residue were sequentially zeroed, roughly in order of the distance between Cα of the residue and the center of the substrate. First, the QM energy of the fully charged system was calculated. Then, after each step of charge deletion, the QM energy was recalculated, and the difference between the energy before and after charge deletion of a residue corresponds to the interaction energy between this residue and the QM region. The results were then averaged, and the interaction energies at the TS and IS relative to the RS were computed. The effect of the enzyme residues on the relative stability of the TS and IS relative to the RS is presented in Figure 8.

The side-chain of Ser83 and the backbones of Ser84, Gly85, Asn86, and His87 interact with the carboxylate group of the Ser-substrate as part of an anion hole. The interaction of the carboxylate with the anion hole helps relieve the electrostatic repulsion between the carboxylate moiety and the negative charge of the pyridine oxyanion and the accumulating δ- on Cα during the reaction. In the RS and at the TS, the substrate Cα still has a near $sp^3$ hybridization (Figure 4), positioning the


DOI: 10.1021/bi500984m
Biochemistry 2015, 54, 516−527

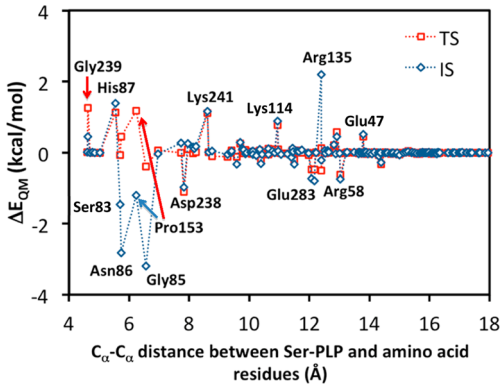


**Figure 8.** Individual residue contributions to stabilization or destabilization of the transition state (red) and the intermediate state (blue) relative to the reactant state (L-Ser-PLP Michaelis complex) as a function of the distance between the C$\alpha$ atoms of L-Ser-PLP and enzyme residues.

carboxylate group close to the amide-moiety of Ser83, Ser84, and His87 (Table 3). For instance, at the TS and IS the His87 moiety has a destabilizing effect of ca. 1 kcal/mol relative to the RS, due to weakening of the H-bond between the amide backbone and the substrate carboxylate. Concomitant with the deprotonation of L-Ser, the carboxylate group moves toward the backbones of Gly85 and Asn86, and the H-bond between the Asn86 side chain and the pyridine oxyanion tightens. The net stabilizing effect of the IS by Gly85 and Asn86 is −3.2 and −2.8 kcal/mol, respectively. Both of these residues stabilize the TS much less than the IS. Similarly, Ser83 has little effect on the TS, but stabilizes the IS by −1.5 kcal/mol.

The backbone carbonyl of Pro153 interacts with the side-chain of the catalytic Lys56 throughout the reaction. This H-bond is weakened at the TS (1.2 kcal/mol) as Lys56 moves away from Pro153 to extract the H$\alpha$ proton, only to strengthen again in the IS as Lys56 becomes positively charged (−1.2 kcal/mol).

The positively charged Arg135 and Lys241 both interact more favorably with the RS than with the TS and IS. Considering that both of these residues are positioned in closer proximity to the carboxylate of the substrate-PLP moiety than to Lys56, we conclude that the active site anion hole stabilizing the substrate carboxylate effectively screens any buildup of negative charge. Additional distal residues that influence the charge transfer during the first reaction step are Arg58, Glu47, and Glu283, although the effect is small. The effect of charged residues on charge migration observed herein mirrors that observed for AlaR in our earlier work.[35]

The subsequent step in the L-Ser → D-Ser reaction (i.e., proton donation by Ser84) entails a similar charge transfer vector and the residues discussed above might be expected to behave in a similar manner. On the other hand, the effect of the distal charged residues discussed above might be reversed for the D-Ser → L-Ser direction. Thus, it seems like one should, at least in principle, be able to shift the equilibrium in favor of L-Ser or D-Ser by generating carefully selected SerR mutant forms. It would therefore be interesting to employ site-directed mutagenesis to scrutinize the effect of the above-mentioned residues on catalysis.

**Docking of Malonate into the Resulting SerR Active Site.** In order to examine the active site obtained from our MD simulations, in comparison with the active site from the original X-ray structure of rat SerR, the original inhibitor, malonate, was extracted from the X-ray structure and docked into the resulting active site at the RS, in its internal aldimine form. Subsequently, the two active sites, in complex with the inhibitor molecules, were superimposed and compared. The structures superimpose well (Figure 9) with an RMSD of 1.21 Å, meaning that the

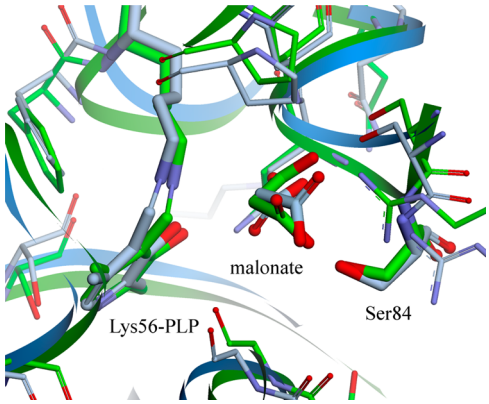


**Figure 9.** Superimposed active sites of the original crystallographic rat SerR (green) and the final rat SerR (light blue).

active site geometry was well preserved throughout our MD simulations. Considering that the simulated form of SerR corresponds to a catalytically active state, we may conclude that the crystal structure with the malonate inhibitor is rather similar to the active form of the enzyme. However, small changes occurred in the active site, which are required to accommodate the substrate in the external aldimine form. Furthermore, the catalytic acid−base pair reorganized in order to facilitate optimal catalysis. The simulated structure may serve as a target for docking studies that might lead to the discovery of new SerR inhibitors.

## 4. SUMMARY

This work describes a combined classical and quantum simulation study of the racemization reaction catalyzed by rat and human SerR. To elucidate the catalytic effect in SerR, we used a QM/MM potential energy surface to describe the breaking and forming of bonds throughout the reaction, and a centroid path integral method to describe nuclear quantum effects. In this work we used the AM1 Hamiltonian with specific reaction parameters that were previously developed for AlaR, and were shown to be accurate for the L-Ser ⇄ D-Ser racemization as well. Our results confirm that in SerR, the reaction occurs via a stepwise mechanism with a distinct intermediate PLP-substrate carbanion species, as in AlaR. Similarly to AlaR, the PLP-substrate intermediate is stabilized mostly due to solvation effects contributed by water molecules and active-site residues, as well as long-range electrostatic interactions with the enzyme environment. When taking into account the binding of Mg·ATP to the enzyme, the free energy barriers obtained for the L-Ser → D-Ser enzymatic reaction, as well as for the reverse reaction, are in good agreement with experimental values. In addition to a deeper understanding of the racemization mechanism in SerR, based on our simulations one might propose specific mutations, which might shift the SerR equilibrium in favor of either L-Ser or D-Ser. Finally, the current studies have produced catalytically competent forms of


DOI: 10.1021/bi500984m
Biochemistry 2015, 54, 516−527

the rat and human enzymes, which may serve as targets for future docking studies and drug design.

## ■ ASSOCIATED CONTENT

### Supporting Information

Coordinates of model complexes and individual molecules calculated using density functional theory and semiempirical methods; geometric constraints applied on the model complexes for gas-phase and solution-phase calculations; calculated and experimental gas-phase proton affinities of model molecules; His protonation states; human SerR two-dimensional CM PMF. This material is available free of charge via the Internet at http://pubs.acs.org.

## ■ AUTHOR INFORMATION


### Corresponding Author

*Phone: 972-3-5317392. E-mail: majort@biu.ac.il.


### Notes

The authors declare no competing financial interest.

## ■ REFERENCES


(1) Walsh, C. (1989) Enzymes in the D-alanine branch of bacterial cell wall peptidoglycan assembly. *J. Biol. Chem. 264*, 2393−2396.

(2) Goto, M., Yamauchi, T., Kamiya, N., Miyahara, I., Yoshimura, T., Mihara, H., Kurihara, T., Hirotsu, K., and Esaki, N. (2009) Crystal structure of a homolog of mammalian serine racemase from *Schizosaccharomyces pombe*. *J. Biol. Chem. 284*, 25944−25952.

(3) Uo, T., Yoshimura, T., Shimizu, S., and Esaki, N. (1998) Occurrence of pyridoxal 5′-phosphate-dependent serine racemase in silkworm *Bombyx mori*. *Biochem. Biophys. Res. Commun. 246*, 31−34.

(4) Fujitani, Y., Nakajima, N., Ishihara, K., Oikawa, T., Ito, K., and Sugimoto, M. (2006) Molecular and biochemical characterization of a serine racemase from *Arabidopsis thaliana*. *Phytochemistry 67*, 668−674.

(5) Fujitani, Y., Horiuchi, T., Ito, K., and Sugimoto, M. (2007) Serine racemases from barley, *Hordeum vulgare* L., and other plant species represent a distinct eukaryotic group: Gene cloning and recombinant protein characterization. *Phytochemistry 68*, 1530−1536.

(6) Gogami, Y., Ito, K., Kamitani, Y., Matsushima, Y., and Oikawa, T. (2009) Occurrence of D-serine in rice and characterization of rice serine racemase. *Phytochemistry 70*, 380−387.

(7) Hashimoto, A., Nishikawa, T., Hayashi, T., Fujii, N., Harada, K., Oka, T., and Takahashi, K. (1992) The presence of free D-serine in rat brain. *FEBS Lett. 296*, 33−36.

(8) Danysz, W., Zajaczkowski, W., and Parsons, C. (1995) Modulation of learning processes by ionotropic glutamate receptor ligands. *Behav. Pharmacol. 6*, 455−474.

(9) Fuziwara, S., Inoue, K., and Denda, M. (2003) NMDA-type glutamate receptor is associated with cutaneous barrier homeostasis. *J. Invest. Dermatol. 120*, 1023−1029.

(10) Nahm, W. K., Philpot, B. D., Adams, M. M., Badiavas, E. V., Zhou, L. H., Butmarc, J., Bear, M. F., and Falanga, V. (2004) Significance of *N*-methyl D-aspartate (NMDA) receptor mediated signaling in human keratinocytes. *J. Cell. Physiol. 200*, 309−317.

(11) Inoue, R., Yoshihisa, Y., Tojo, Y., Okamura, C., Yoshida, Y., Kishimoto, J., Luan, X., Watanabe, M., Mizuguchi, M., and Nabeshima, Y. (2014) Localization of serine racemase and its role in the skin. *J. Invest. Dermatol. 134*, 1618−1626.

(12) Schell, M. J., Molliver, M. E., and Snyder, S. H. (1995) D-Serine, an endogenous synaptic modulator: localization to astrocytes and glutamate-stimulated release. *Proc. Natl. Acad. Sci. U. S. A. 92*, 3948−3952.

(13) Hashimoto, A., Nishikawa, T., Oka, T., and Takahashi, K. (1993) Endogenous D-serine in rat brain: *N*-methyl-D-aspartate receptor-related distribution and aging. *J. Neurochem. 60*, 783−786.

(14) Mothet, J.-P., Parent, A. T., Wolosker, H., Brady, R. O., Linden, D. J., Ferris, C. D., Rogawski, M. A., and Snyder, S. H. (2000) D-serine is an endogenous ligand for the glycine site of the *N*-methyl-D-aspartate receptor. *Proc. Natl. Acad. Sci. U. S. A. 97*, 4926−4931.

(15) Wolosker, H., Blackshaw, S., and Snyder, S. H. (1999) Serine racemase: a glial enzyme synthesizing D-serine to regulate glutamate-*N*-methyl-D-aspartate neurotransmission. *Proc. Natl. Acad. Sci. U. S. A. 96*, 13409−13414.

(16) Bräuner-Osborne, H., Egebjerg, J., Nielsen, E. Ø., Madsen, U., and Krogsgaard-Larsen, P. (2000) Ligands for glutamate receptors: design and therapeutic prospects. *J. Med. Chem. 43*, 2609−2645.

(17) Krystal, J. H., Karper, L. P., Seibyl, J. P., Freeman, G. K., Delaney, R., Bremner, J. D., Heninger, G. R., Bowers, M. B., Jr, and Charney, D. S. (1994) Subanesthetic effects of the noncompetitive NMDA antagonist, ketamine, in humans: psychotomimetic, perceptual, cognitive, and neuroendocrine responses. *Arch. Gen. Psychiatr. 51*, 199.

(18) Kemp, J. A., and McKernan, R. M. (2002) NMDA receptor pathways as drug targets. *Nat. Neurosci. 5*, 1039−1042.

(19) Mori, H., Wada, R., Li, J., Ishimoto, T., Mizuguchi, M., Obita, T., Gouda, H., Hirono, S., and Toyooka, N. (2014) In silico and pharmacological screenings identify novel serine racemase inhibitors. *Bioorg. Med. Chem. Lett. 24*, 3732−3735.

(20) Vorlová, B., Nachtigallová, D., Jirásková-Vaníčková, J., Ajani, H., Jansa, P., Řezáč, J., Fanfrlík, J., Otyepka, M., Hobza, P., and Konvalinka, J. (2014) Malonate-based inhibitors of mammalian serine racemase: Kinetic characterization and structure-based computational study. *Eur. J. Med. Chem. 89*, 189−197.

(21) De Miranda, J., Panizzutti, R., Foltyn, V. N., and Wolosker, H. (2002) Cofactors of serine racemase that physiologically stimulate the synthesis of the *N*-methyl-D-aspartate (NMDA) receptor coagonist D-serine. *Proc. Natl. Acad. Sci. U. S. A. 99*, 14542−14547.

(22) Stříšovskỳ, K., Jirásková, J., Bařinka, C., Majer, P., Rojas, C., Slusher, B. S., and Konvalinka, J. (2003) Mouse brain serine racemase catalyzes specific elimination of L-serine to pyruvate. *FEBS Lett. 535*, 44-−48.

(23) Yoshimura, T., and Goto, M. (2008) D-Amino acids in the brain: structure and function of pyridoxal phosphate-dependent amino acid racemases. *FEBS J. 275*, 3527−3537.

(24) Smith, M. A., Mack, V., Ebneth, A., Moraes, I., Felicetti, B., Wood, M., Schonfeld, D., Mather, O., Cesura, A., and Barker, J. (2010) The structure of mammalian serine racemase: Evidence for conformational changes upon inhibitor binding. *J. Biol. Chem. 285*, 12873−12881.

(25) Watanabe, A., Kurokawa, Y., Yoshimura, T., and Esaki, N. (1999) Role of tyrosine 265 of alanine racemase from *Bacillus stearothermophilus*. *J. Biochem. 125*, 987−990.

(26) Watanabe, A., Kurokawa, Y., Yoshimura, T., Kurihara, T., Soda, K., and Esaki, N. (1999) Role of lysine 39 of alanine racemase from *Bacillus stearothermophilus* that binds pyridoxal 5′-phosphate. *J. Biol. Chem. 274*, 4189−4194.

(27) Watanabe, A., Yoshimura, T., Mikami, B., Hayashi, H., Kagamiyama, H., and Esaki, N. (2002) Reaction mechanism of alanine racemase from *Bacillus stearothermophilus*. *J. Biol. Chem. 277*, 19166−19172.

(28) Eliot, A. C., and Kirsch, J. F. (2004) Pyridoxal phosphate enzymes: mechanistic, structural, and evolutionary considerations. *Annu. Rev. Biochem. 73*, 383−415.

(29) Sharif, S., Huot, M. C., Tolstoy, P. M., Toney, M. D., Jonsson, K. H. M., and Limbach, H.-H. (2007) $^{15}$N nuclear magnetic resonance studies of acid-base properties of pyridoxal-5′-phosphate aldimines in aqueous solution. *J. Phys. Chem. B 111*, 3869−3876.

(30) Bruice, T. C., Fife, T. H., Bruno, J., and Brandon, N. E. (1962) Hydroxyl group catalysis. II. The reactivity of the hydroxyl group of serine. The nucleophilicity of alcohols and the ease of hydrolysis of their acetyl esters as related to their p$K_a$. *Biochemistry 1*, 7−12.

(31) Griswold, W. R., and Toney, M. D. (2011) Role of the pyridine nitrogen in pyridoxal 5′-phosphate catalysis: activity of three classes of




DOI: 10.1021/bi500984m
*Biochemistry* 2015, 54, 516−527

PLP enzymes reconstituted with deazapyridoxal 5′-phosphate. *J. Am. Chem. Soc. 133*, 14823−14830.
(32) Richard, J. P., Amyes, T. L., Crugeiras, J., and Rios, A. (2009) Pyridoxal 5′-phosphate: electrophilic catalyst extraordinaire. *Curr. Opin. Chem. Biol. 13*, 475−483.
(33) Caulkins, B. G., Bastin, B., Yang, C., Neubauer, T. J., Young, R. P., Hilario, E., Huang, Y.-m. M., Chang, C.-e. A., Fan, L., Dunn, M. F., Marsella, M. J., and Mueller, L. J. (2014) Protonation States of the Tryptophan Synthase Internal Aldimine Active Site from Solid-State NMR Spectroscopy: Direct Observation of the Protonated Schiff Base Linkage to Pyridoxal-5′-Phosphate. *J. Am. Chem. Soc. 136*, 12824−12827.
(34) Major, D. T., Nam, K., and Gao, J. (2006) Transition state stabilization and $\alpha$-amino carbon acidity in alanine racemase. *J. Am. Chem. Soc. 128*, 8114−8115.
(35) Major, D. T., and Gao, J. (2006) A combined quantum mechanical and molecular mechanical study of the reaction mechanism and $\alpha$-amino acidity in alanine racemase. *J. Am. Chem. Soc. 128*, 16345−16357.
(36) Rubinstein, A., and Major, D. T. (2010) Understanding catalytic specificity in alanine racemase from quantum mechanical and molecular mechanical simulations of the arginine 219 mutant. *Biochemistry 49*, 3957−3964.
(37) Lin, Y.-L., Gao, J., Rubinstein, A., and Major, D. T. (2011) Molecular dynamics simulations of the intramolecular proton transfer and carbanion stabilization in the pyridoxal 5′-phosphate dependent enzymes l-dopa decarboxylase and alanine racemase. *Biochim. Biophys. Acta 1814*, 1438−1446.
(38) Warshel, A., and Levitt, M. (1976) Theoretical studies of enzymic reactions: dielectric, electrostatic and steric stabilization of the carbonium ion in the reaction of lysozyme. *J. Mol. Biol. 103*, 227−249.
(39) Field, M. J., Bash, P. A., and Karplus, M. (1990) A combined quantum mechanical and molecular mechanical potential for molecular dynamics simulations. *J. Comput. Chem. 11*, 700−733.
(40) Gao, J. (1996) Methods and applications of combined quantum mechanical and molecular mechanical potentials. *Rev. Comput. Chem. 7*, 119−186.
(41) Torrie, G. M., and Valleau, J. P. (1977) Nonphysical sampling distributions in Monte Carlo free-energy estimation: Umbrella sampling. *J. Comput. Phys. 23*, 187−199.
(42) Kästner, J. (2011) Umbrella sampling. *Wiley Interdiscip. Rev. Comput. Mol. Sci. 1*, 932−942.
(43) Zhao, Y., and Truhlar, D. G. (2008) The M06 suite of density functionals for main group thermochemistry, thermochemical kinetics, noncovalent interactions, excited states, and transition elements: two new functionals and systematic testing of four M06-class functionals and 12 other functionals. *Theor. Chem. Acc. 120*, 215−241.
(44) Adamo, C., and Barone, V. (1998) Exchange functionals with improved long-range behavior and adiabatic connection methods without adjustable parameters: The mPW and mPW1PW models. *J. Chem. Phys. 108*, 664.
(45) Hehre, W. J., Radom, L., Schleyer, P. R., and Pople, J. A. (1986) *Ab Initio Molecular Orbital Theory*; John Wiley & Sons, New York.
(46) Dewar, M. J., Zoebisch, E. G., Healy, E. F., and Stewart, J. J. (1985) Development and use of quantum mechanical molecular models. 76. AM1: a new general purpose quantum mechanical molecular model. *J. Am. Chem. Soc. 107*, 3902−3909.
(47) Puig, E., Mixcoha, E., Garcia-Viloca, M., González-Lafont, A., and Lluch, J. M. (2009) How the substrate D-glutamate drives the catalytic action of *Bacillus subtilis* glutamate racemase. *J. Am. Chem. Soc. 131*, 3509−3521.
(48) Rubinstein, A., and Major, D. T. (2009) Catalyzing racemizations in the absence of a cofactor: The reaction mechanism in proline racemase. *J. Am. Chem. Soc. 131*, 8513−8521.
(49) Cancès, E., Mennucci, B., and Tomasi, J. (1997) A new integral equation formalism for the polarizable continuum model: Theoretical background and applications to isotropic and anisotropic dielectrics. *J. Chem. Phys. 107*, 3032−3041.
(50) Mennucci, B., Cancès, E., and Tomasi, J. (1997) Evaluation of solvent effects in isotropic and anisotropic dielectrics and in ionic solutions with a unified integral equation method: Theoretical bases, computational implementation, and numerical applications. *J. Phys. Chem. B 101*, 10506−10517.
(51) Mennucci, B., and Tomasi, J. (1997) Continuum solvation models: A new approach to the problem of solute's charge distribution and cavity boundaries. *J. Chem. Phys. 106*, 5151−5158.
(52) Tomasi, J., Mennucci, B., and Cances, E. (1999) The IEF version of the PCM solvation method: an overview of a new method addressed to study molecular solutes at the QM ab initio level. *J. Mol. Struct. 464*, 211−226.
(53) R. A, Frisch, M. J.; Trucks, G. W.; Schlegel, H. B.; Scuseria, G. E.; Robb, M. A.; Cheeseman, J. R.; Scalmani, G.; Barone, V.; Mennucci, B.; Petersson, G. A.; Nakatsuji, H.; Caricato, M.; Li, X.; Hratchian, H. P.; Izmaylov, A. F.; Bloino, J.; Zheng, G.; Sonnenberg, J. L.; Hada, M.; Ehara, M.; Toyota, K.; Fukuda, R.; Hasegawa, J.; Ishida, M.; Nakajima, T.; Honda, Y.; Kitao, O.; Nakai, H.; Vreven, T.; Montgomery, J. A.; , Jr., Peralta, J. E.; Ogliaro, F.; Bearpark, M.; Heyd, J. J.; Brothers, E.; Kudin, K. N.; Staroverov, V. N.; Kobayashi, R.; Normand, J.; Raghavachari, K.; Rendell, A.; Burant, J. C.; Iyengar, S. S.; Tomasi, J.; Cossi, M.; Rega, N.; Millam, J. M.; Klene, M.; Knox, J. E.; Cross, J. B.; Bakken, V.; Adamo, C.; Jaramillo, J.; , . Gomperts, R. E. Stratmann, O. Yazyev, A. J. Austin, R. Cammi, C. Pomelli, J. W. Ochterski, R. L. Martin, K. Morokuma, V. G. Zakrzewski, G. A. Voth, P. Salvador, J. J. Dannenberg, S. Dapprich, A. D. Daniels, O. Farkas, J. B. Foresman, J. V. Ortiz, J. Cioslowski, and Fox, D. J. (2009) *Gaussian 09*, Gaussian, Inc., Wallingford CT, .
(54) Cook, S. P., Galve-Roperh, I., del Pozo, Á. M. n., and Rodríguez-Crespo, I. (2002) Direct calcium binding results in activation of brain serine racemase. *J. Biol. Chem. 277*, 27782−27792.
(55) Neidle, A., and Dunlop, D. S. (2002) Allosteric regulation of mouse brain serine racemase. *Neurochem. Res. 27*, 1719−1724.
(56) Gogami, Y., Kobayashi, A., Ikeuchi, T., and Oikawa, T. (2010) Site directed mutagenesis of rice serine racemase: evidence that Glu219 and Asp225 mediate the effects of $Mg^{2+}$ on the activity. *Chem. Biodivers. 7*, 1579−1590.
(57) Marchetti, M., Bruno, S., Campanini, B., Bettati, S., Peracchi, A., and Mozzarelli, A. (2014) Regulation of human serine racemase activity and dynamics by halides, ATP and malonate. *Amino Acids*, 1−11.
(58) Brooks, B. R., Bruccoleri, R. E., Olafson, B. D., Swaminathan, S., and Karplus, M. (1983) CHARMM: A program for macromolecular energy, minimization, and dynamics calculations. *J. Comput. Chem. 4*, 187−217.
(59) Brooks, B. R., Brooks, C. L., MacKerell, A. D., Nilsson, L., Petrella, R. J., Roux, B., Won, Y., Archontis, G., Bartels, C., and Boresch, S. (2009) CHARMM: the biomolecular simulation program. *J. Comput. Chem. 30*, 1545−1614.
(60) Allen, M. P., and Tildesley, D. J. (1989) *Computer Simulation of Liquids*, Oxford University Press, Oxford, U.K.
(61) Gao, J., Amara, P., Alhambra, C., and Field, M. J. (1998) A generalized hybrid orbital (GHO) method for the treatment of boundary atoms in combined QM/MM calculations, *J. Phys. Chem. A 102*, 4714−4721.
(62) MacKerell, A. D., Banavali, N., and Foloppe, N. (2000) Development and current status of the CHARMM force field for nucleic acids. *Biopolymers 56*, 257−265.
(63) MacKerell, A. D., Bashford, D., Bellott, M., Dunbrack, R., Evanseck, J., Field, M. J., Fischer, S., Gao, J., Guo, H., and Ha, S. a. (1998) All-atom empirical potential for molecular modeling and dynamics studies of proteins. *J. Phys. Chem. B 102*, 3586−3616.
(64) Best, R. B., Zhu, X., Shim, J., Lopes, P. E., Mittal, J., Feig, M., and MacKerell, A. D., Jr (2012) Optimization of the additive CHARMM all-atom protein force field targeting improved sampling of the backbone $\phi$, $\psi$ and side-chain $\chi_1$ and $\chi_2$ dihedral angles. *J. Chem. Theory Comput. 8*, 3257−3273.


DOI: 10.1021/bi500984m
*Biochemistry* 2015, 54, 516−527

(65) Northrup, S. H., Pear, M. R., Lee, C.-Y., McCammon, J. A., and Karplus, M. (1982) Dynamical theory of activated processes in globular proteins. *Proc. Natl. Acad. Sci. U. S. A. 79*, 4035−4039.
(66) Kottalam, J., and Case, D. A. (1988) Dynamics of ligand escape from the heme pocket of myoglobin. *J. Am. Chem. Soc. 110*, 7690−7697.
(67) Pu, J., Ma, S., Garcia-Viloca, M., Gao, J., Truhlar, D. G., and Kohen, A. (2005) Nonperfect synchronization of reaction center rehybridization in the transition state of the hydride transfer catalyzed by dihydrofolate reductase. *J. Am. Chem. Soc. 127*, 14879−14886.
(68) Doron, D., Kohen, A., and Major, D. T. (2012) Collective reaction coordinate for hybrid quantum and molecular mechanics simulations: A case study of the hydride transfer in dihydrofolate reductase. *J. Chem. Theory Comput. 8*, 2484−2496.
(69) Vardi-Kilshtain, A., Doron, D., and Major, D. T. (2013) Quantum and classical simulations of orotidine monophosphate decarboxylase: support for a direct decarboxylation mechanism. *Biochemistry 52*, 4382−4390.
(70) Bartels, C., and Karplus, M. (1997) Multidimensional adaptive umbrella sampling: applications to main chain and side chain peptide conformations. *J. Comput. Chem. 18*, 1450−1462.
(71) Kumar, S., Rosenberg, J. M., Bouzida, D., Swendsen, R. H., and Kollman, P. A. (1992) The weighted histogram analysis method for free-energy calculations on biomolecules. I. The method. *J. Comput. Chem. 13*, 1011−1021.
(72) Weinan, E., Ren, W., and Vanden-Eijnden, E. (2007) Simplified and improved string method for computing the minimum energy paths in barrier-crossing events. *J. Chem. Phys. 126*, 164103.
(73) Nam, K., Gao, J., and York, D. M. (2005) An efficient linear-scaling Ewald method for long-range electrostatic interactions in combined QM/MM calculations. *J. Chem. Theory Comput. 1*, 2−13.
(74) Hwang, J., Chu, Z., Yadav, A., and Warshel, A. (1991) Simulations of quantum mechanical corrections for rate constants of hydride-transfer reactions in enzymes and solutions. *J. Phys. Chem. 95*, 8445−8448.
(75) Hwang, J. K., and Warshel, A. (1993) A quantized classical path approach for calculations of quantum mechanical rate constants. *J. Phys. Chem. 97*, 10053−10058.
(76) Major, D. T., and Gao, J. (2005) Implementation of the bisection sampling method in path integral simulations. *J. Mol. Graphics Modell. 24*, 121−127.
(77) Major, D. T., and Gao, J. (2007) An integrated path integral and free-energy perturbation-umbrella sampling method for computing kinetic isotope effects of chemical reactions in solution and in enzymes. *J. Chem. Theory Comput. 3*, 949−960.
(78) Major, D. T., Garcia-Viloca, M., and Gao, J. (2006) Path integral simulations of proton transfer reactions in aqueous solution using combined QM/MM potentials. *J. Chem. Theory Comput. 2*, 236−245.
(79) Wolosker, H., Sheth, K. N., Takahashi, M., Mothet, J.-P., Brady, R. O., Ferris, C. D., and Snyder, S. H. (1999) Purification of serine racemase: biosynthesis of the neuromodulator D-serine. *Proc. Natl. Acad. Sci. U. S. A. 96*, 721−725.
(80) Foltyn, V. N., Bendikov, I., De Miranda, J., Panizzutti, R., Dumin, E., Shleper, M., Li, P., Toney, M. D., Kartvelishvily, E., and Wolosker, H. (2005) Serine racemase modulates intracellular D-serine levels through an $\alpha,\beta$-elimination activity. *J. Biol. Chem. 280*, 1754−1763.
(81) Major, D. T., Heroux, A., Orville, A. M., Valley, M. P., Fitzpatrick, P. F., and Gao, J. (2009) Differential quantum tunneling contributions in nitroalkane oxidase catalyzed and the uncatalyzed proton transfer reaction. *Proc. Natl. Acad. Sci. U. S. A. 106*, 20734−20739.
(82) Bernasconi, C. F. (1992) The principle of nonperfect synchronization: more than a qualitative concept? *Acc. Chem. Res. 25*, 9−16.
(83) Jiraskova-Vanickova, J., Ettrich, R., Vorlova, B., E Hoffman, H., Lepsik, M., Jansa, P., and Konvalinka, J. (2011) Inhibition of human serine racemase, an emerging target for medicinal chemistry. *Curr. Drug Targets 12*, 1037−1055.
(84) Bash, P. A., Field, M. J., Davenport, R., Petsko, G. A., Ringe, D., and Karplus, M. (1991) Computer simulation and analysis of the reaction pathway of triosephosphate isomerase. *Biochemistry 30*, 5826−5832.
(85) Garcia-Viloca, M., Truhlar, D. G., and Gao, J. (2003) Reaction-path energetics and kinetics of the hydride transfer reaction catalyzed by dihydrofolate reductase. *Biochemistry 42*, 13558−13575.
(86) Hensen, C., Hermann, J. C., Nam, K., Ma, S., Gao, J., and Höltje, H.-D. (2004) A combined QM/MM approach to protein-ligand interactions: polarization effects of the HIV-1 protease on selected high affinity inhibitors. *J. Med. Chem. 47*, 6673−6680.


DOI: 10.1021/bi500984m
*Biochemistry* 2015, 54, 516−527